2013 IEEE/RSJ International Conference on
Intelligent Robots and Systems (IROS)
November 3-7, 2013. Tokyo, Japan

Performance Analysis and Characterization of Bio-Inspired Whisker Sensors for Underwater Applications

Pablo Valdivia y Alvarado[1,2], Vignesh Subramaniam[1], and Michael Triantafyllou[1,2]

Abstract— **Pinnipeds (seals, sea lions, etc.) use their whiskers to find and track hydrodynamic trails left by potential prey. Our group recently developed new underwater sensors based on pinniped whiskers, which not only exploit their characteristic geometries but also the dynamics of whisker follicles to improve and tailor sensing capabilities. The sensors are simple, robust, and a straightforward methodology can be used to tailor their sensitivity to different target signals. A lumped parameter model is used to predict sensor performance. The model predictions for static scenarios are compared to experimental results for constant speed measurements. Scalings for static and dynamic measurement scenarios are also given. In both cases the sensors show a strong sensitivity to follicle material properties and whisker length. The results show the sensors can be used for flow sensing and are a promising feedback source for navigation based on near field hydrodynamic features.**

I. INTRODUCTION

Underwater vehicles rely on their ability to sense position, velocity, acceleration, and obstacle locations to properly navigate. The ability of identifying hydrodynamic conditions of interest such as wakes or currents can further enable efficient path planning while exploiting favorable environment dynamics [1]. Traditionally, underwater vehicles use inertial measurement units (IMUs), GPS (when on the surface), sonar, and acoustic doppler current profilers (ADCPs) to measure or estimate all navigation parameters. Apart from their physical limitations, traditional sensors often generate data too large to be handled in real-time in vehicles with limited computing power. Sonar and ADCP data is often post-processed and used for surveys where the information is analyzed after a mission is completed. Additional processing steps are required to sufficiently reduce data size for real-time feedback. As missions require more system components that compete for the limited power and computing resources on board autonomous vehicles, simple sensors that can provide information-rich data manageable in real-time are needed to improve feedback and planning tasks.

Knowledge of the environment conditions around a vehicle is also important when assessing hydrodynamic constraints for path planning. Sonar and ADCP data provide information for regions surrounding a vehicle but not immediately adjacent to it. In contrast, it is believed that fish and other marine species infer information about their surroundings from data gathered at close proximity [2].

To better understand the impact on vehicle maneuverability of hydrodynamic sensing at proximity our group is studying different approaches to biomimetic underwater sensing. In the present work the performance of a sensor based on pinniped whiskers is analyzed. Pinnipeds track prey using only information provided by their whiskers. They can successfully locate tracks even several minutes after a prey has passed by [3]. This feat is even more remarkable given that thin elongated structures such as whiskers are expected to develop vortex induced vibrations (VIV) as they are dragged through a liquid medium. The resulting uncontrolled vibrations would present an underlaying noise that would severely interfere with measurements. In the case of pinniped whiskers, their unique geometry which involves lengthwise undulations seems to minimize or eliminate VIV [4], [5]. Without the threat of flow induced noise, these apparently simple systems are capable of high sensitivities to environmental perturbations. This level of sensitivity could enable numerous underwater applications for path planning and tracking using favorable hydrodynamics. The sensors presented in this study use pinniped whisker particular geometries while also exploiting the dynamic properties of their follicles. Their sensing dynamics are analyzed and simple models are presented that can be used to tailor measurements for signals of interest.

II. PRIOR ART

Sensing nearby fluid dynamics is important for underwater navigation. Unfortunately, traditional flow sensing methods do not provide required sensitivity or range. Previous studies have looked at alternative flow sensors that exploit hair-like structure interactions with the environment mimicking fish lateral line neuromasts and arthropod filiform hairs [6]. Sensing structures fall in the millimeter to micron range and their fluid driven deformations are measured using piezoresistive, capacitive, magnetic, or piezoelectric transducers. Examples of piezoresistive cantilever supported hair-like structures mimicking fish neuromasts along with their performance are described in [7], [8], [9]. Some examples of capacitive hair sensors include [10], [11], [12]. Tao [6] reviews recent advances in this area both in terms of theoretical understanding and device design. Reported fluid velocity measurement sensitivities are in the order of mm/s.

*This work was funded in whole or in part by the Singapore National Research Foundation (NRF) through the Singapore-MIT Alliance for Research and Technology (SMART).

[1,2]P. Valdivia y Alvarado and M. Triantafyllou are with the Center for Environmental Sensing and Modeling, Singapore-MIT Alliance for Research and Technology, Singapore 138602, and the Department of Mechanical Engineering, Massachusetts Institute of Technology, Cambridge, MA 02139, USA `pablov at mit.edu, mistetri at mit.edu`

[1]V. Subramaniam is with the Center for Environmental Sensing and Modeling, Singapore-MIT Alliance for Research and Technology, Singapore 138602 `vignesh at smart.mit.edu`

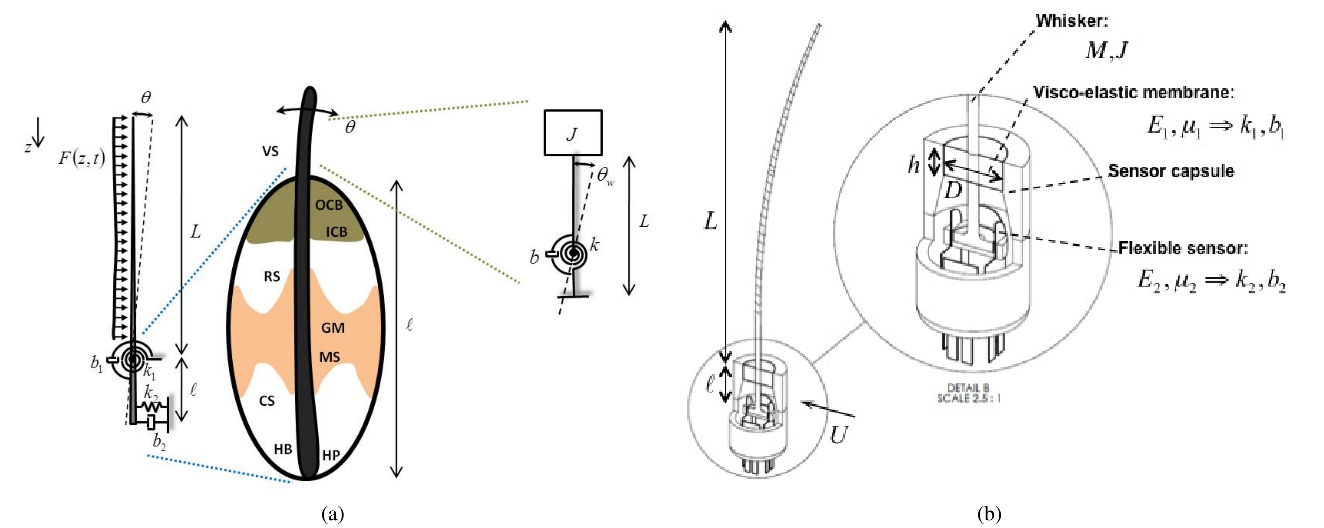

Fig. 1. (a) Whisker-FSC system: The bending deflections θ_w of a whisker-shaft of length L can be modeled by a spring-inertia-damper lumped parameter model (k, J, b). Its supporting FSC of length ℓ is modeled by a torsional spring-damper system (k_1, b_1) in parallel with a linear spring-damper system (k_2, b_2). (b) Basic whisker-like sensor design: A whisker-like shaft is supported by a visco-elastic membrane with modulus E_1 and viscosity μ_1. Flexible displacement sensors with modulus E_2 and viscosity μ_2 detect whisker base oscillations θ.

Large scale hair-like sensor studies for underwater applications are in contrast scarcer. Rodent whiskers have been studied and implemented in land autonomous vehicles, but their sensing mechanism involves physical contact with solid surfaces and present different dynamics than the underwater case. For underwater applications, Stocking et al. [13] and Eberhardt et al. [14] proposed whisker-like sensors that used capacitance changes in a "cone in cone" base to measure fluid motion. Solomon [15] used steel whiskers fitted with strain gauges to provide surface (and potentially hydrodynamic) measurements. None of the whisker-shafts used in these sensors exploited the particular geometry found in pinniped whiskers and were likely at risk of developing VIV. The few studies involving large scale whisker-like sensors to date have concentrated on single designs and little effort was given to provide guidelines to characterize and tailor sensor performance. Further, in all previous studies, sensor robustness for practical field applications is rarely analyzed or even a concern. MEMS based sensors tend to be stiff and brittle and exposed structural components (such as hair-like structures) can easily be damaged by impacts.

Our group proposed the design of whisker-like sensors based on pinniped whiskers [5]. These large scale sensors have in contrast relatively low structural stiffnesses and can accommodate impacts more easily during field deployments. In this study the sensor theoretical behavior is analyzed in more depth and model parameters as well as sensing performance are characterized and compared to model predictions.

III. WHISKER SENSOR MODEL

Pinnipeds are equipped with several rows of whiskers that grow on each side of their upper lips in surfaces known as vibrissal pads. Each individual whisker shaft is supported by a tissue cluster rich in nerve endings known as the follicle sinus complex (FSC). Fig. 1(a) shows a sketch of the main FSC components (more details in [5]). The bending deflections θ_w of the whisker tip relative to its base can be modeled by a spring-inertia-damper system (with spring constant k, damping coefficient b, and inertia J) shown at the right of Fig. 1(a) (higher order deformations would require more lumped parameters). The FSC support of the whisker shaft can be modeled by a set of springs (with spring constants k_1 and k_2) and dampers (with damping coefficients b_1 and b_2) as shown on Fig. 1(a) which allow rigid body deflections θ at the whisker base [5]. The whisker shaft is composed of keratin with a modulus E_w in the order of 4 (GPa) [16]. In contrast, the FSC tissue has an average modulus E_{FSC} of 10 (kPa) [17]. As a result the whisker stiffness k is orders of magnitude larger than the FSC's combined stiffness and the whisker shaft can be assumed to oscillate as a rigid body ($\theta_w = 0$). When excited by distributed forces $F(z,t)$ due to fluid interactions in a given plane the whisker-FSC dynamics can be modeled by a transfer function of the form,

$$\theta(s) = \frac{L/2}{Js^2 + (b_1 + b_2\ell^2)s + (k_1 + k_2\ell^2)} F(s), \qquad (1)$$

where the inertia term J includes added mass effects. Equation (1) assumes no higher order modes are excited within the whisker structure and differs by a factor of $1/2$ with the transfer function used in [5] to better account for the torque due to the distributed force (the assumption is that the whisker shaft center of mass is located roughly at $L/2$).

Fig. 1(b) shows the basic whisker sensor design. A whisker of length $L+\ell$ and inertia J is supported by a sensor capsule of length ℓ which emulates the FSC. The sensor capsule has a thick but flexible visco-elastic membrane of modulus E_1 and viscosity μ_1 that supports the whisker shaft and constrains its motions. Inside the capsule, four flexible displacement sensors, with modulus E_2 and viscosity μ_2, are preloaded

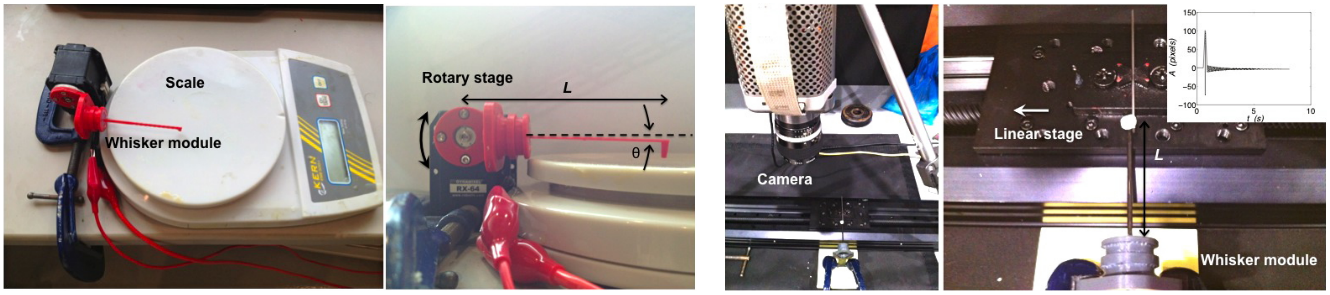

(a) (b)

Fig. 2. FSC system identification experiments. (a) Whisker module mounted in a rotational stage (Dynamixel RX-64 servo) applies increasing loads to a weighing scale (Kern EMB 5.2K1, 5200g weighing capacity, 1g resolution). (b) Whisker module mounted on a linear stage (Zaber T-LST1000D) is perturbed by a stage impulse and the resulting oscillations are recorded to determine the settling time (measured impulse response example shown in inset).

to the base of the whisker to measure its oscillations θ in two perpendicular planes (along and across the direction of motion). The flexible sensors consist of a coated substrate that displays changes in electrical conductivity as it is bent [18]. Equation (1) describes the dynamics of a forced damped oscillator and solutions for both static deflections and dynamic oscillations can be derived from it.

For the static loading case, we assume a uniform constant load F is applied along the whisker. In the absence of VIV, for a whisker with projected area A immersed in uniform flow of density ρ and moving at a speed U, the load F is primarily a result of form drag, $F = \frac{1}{2}\rho U^2 c_d A$, where c_d is the whisker drag coefficient in the plane of motion. Additionally, calibration of the flexible displacement sensors provides a relationship between sensor output voltage v and whisker deflection θ of the form $v = C\theta\ell$, where C is a calibration constant. From (1), for steady state continuous signal inputs (DC case), the sensor should provide measurements of the form,

$$v = \frac{C\ell L\rho U^2 c_d A}{4(k_1 + k_2\ell^2)}. \tag{2}$$

For time varying loads (AC case) of the form $F(t) = F_0 \sin(\omega t)$ (here time varying loads with a dominant frequency ω are assumed for simplicity), the sensor measurements should instead follow the relation,

$$v(t) = \frac{C\ell F_0}{\sqrt{(k_1 + k_2\ell^2 - J\omega^2)^2 + \omega^2(b_1 + b_2\ell^2)^2}} \sin(\omega t + \phi), \tag{3}$$

where $\phi = \arctan\left(\frac{J\omega(b_1+b_2\ell^2)\sqrt{\frac{k_1+k_2\ell^2}{J}}}{\sqrt{J(k_1+k_2\ell^2)}(J\omega^2-(k_1+k_2\ell^2))}\right)$. The membrane and flexible sensor material properties can be chosen to give the whisker sensors a resonant frequency close to the frequency of the expected measurements to amplify them and achieve a high signal to noise ratio. The sensor resonant frequency f_r is given by,

$$f_r \approx \frac{1}{2\pi}\sqrt{\frac{k_1 + k_2\ell^2}{J}}\sqrt{1 - \frac{(b_1 + b_2\ell^2)^2}{2J(k_1 + k_2\ell^2)}} \tag{4}$$

Equations (2), (3), and (4) can be used to both predict the sensor performance and as design guidelines. For a given sensor geometry simple models to identify the corresponding lumped parameters are hence needed. The visco-elastic membrane of diameter D and thickness h provides rotational stiffness and damping to the whisker oscillations, and from beam theory both values can be approximated by,

$$b_1 \approx \frac{n\mu_1 I}{h}, \quad k_1 \approx \frac{nE_1 I}{h} \tag{5}$$

where I is the membrane's second moment of area and n is a constant dependent of the membrane boundary conditions. Here we assume the visco-elastic membrane has thickness and diameter that are of the same order (h is $O(D)$ where $O(X)$ implies a quantity in the order of magnitude of X). In the current design, the flexible displacement sensors display negligible damping ($b_2 \approx 0$) and low stiffness ($k_2 = 0.1N/m$). From (2) and (5) the sensor measurements in the DC case can be shown to scale as,

$$v \sim \frac{hL^3 r\rho U^2}{E_1 D^4} \tag{6}$$

The validity of (1) as a simple model of the whisker sensor dynamics was based on the assumption that the whisker displayed a much larger flexural rigidity than the FSC so that dynamics during normal sensor operation would be dominated by the FSC viscoelasticity with the whisker shaft acting as a rigid body. Using the stiffness approximation in (5) the stiffness ratio between whisker shaft and FSC can be written as,

$$\frac{k}{k_1} = k^* \approx \frac{E_w I_w h}{E_1 I L} \tag{7}$$

where I_w and I are the whisker shaft and FSC second moment of areas which are $O(d^4)$ and $O(D^4)$ respectively and the flexible sensor stiffness is assumed to be negligible compared to the FSC's. Therefore k^* is $O(\frac{E_w d^4 h}{E_1 D^4 L})$ and (1) as well as the analysis presented in this section is applicable provided $k^* >> 1$.

IV. EXPERIMENTS

FSC characterization

Two experiments were performed to test the validity of the expressions in (5). A whisker module was mounted to a rotary servo to apply controlled loads to a scale. The servo

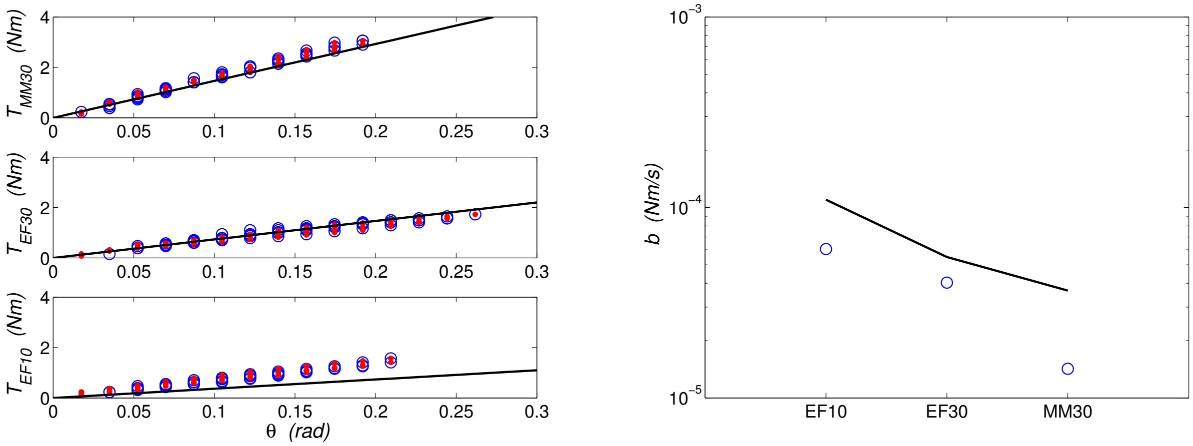

(a) (b)

Fig. 3. FSC system identification results: (a) Measured torques T vs. planar whisker angular deflection θ (blue circles and red dots) plotted against model based on (5) (black line). (b) Measured damping coefficients (blue circles, based on (8)) vs. estimated values (black line, based on (5)) for three different membrane materials.

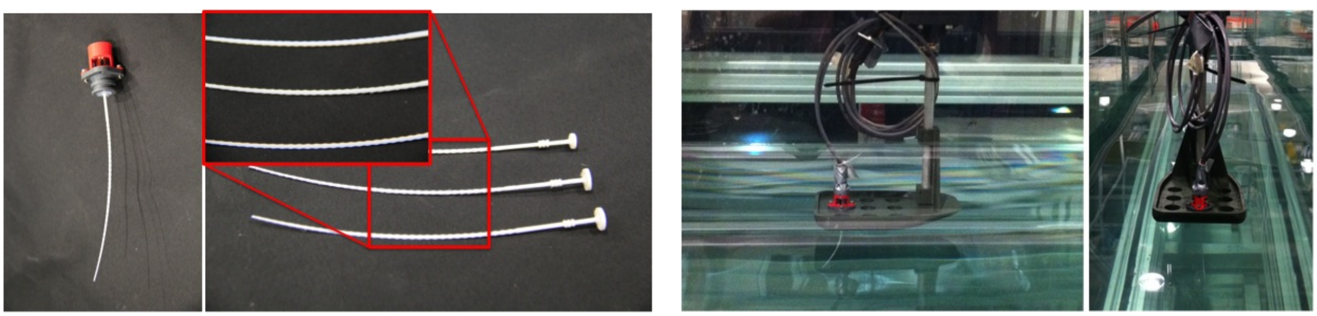

(a) (b)

Fig. 4. (a) Whisker prototype: A polycarbonate whisker is supported inside an artificial FSC. Three whisker shafts are shown along with a close up of the undulations along the shaft length. (b) Whisker carriage: Whisker modules were mounted on a carriage and towed at constant speeds along a 10m x 2m x 1.5m water tank. The carriage kept the whisker modules submerged underwater at all times.

was used to rotate the whisker towards the scale and away from it in small angle increments. At each angle step θ the load F measured by the scale was recorded and the corresponding torque T was determined by multiplying F by the moment arm (length of whisker shaft). The torque versus whisker rotation angle provided an estimate of the FSC rotational stiffness, $k_i = T/\theta$. A second experiment used a linear stage to apply an initial perturbation to the tip of a whisker module, the resulting decaying oscillations were recorded and used to identify the settling time t_s of a given whisker module. The damping coefficients b_i were estimated using the relation,

$$b_i = 8J/t_s. \tag{8}$$

Fig. 2 shows pictures of both experiment setups. Fig. 2(a) shows the whisker module and scale setup (with a shortened whisker to minimize whisker shaft deflections during loading) and Fig. 2(b) shows the whisker module mounted perpendicularly next to a linear stage. The linear stage moves a pin at a speed of 0.16m/s against the whisker shaft and provides the initial impulse. The inset shows the oscillatory response recorded in a single experiment. Fig. 3 shows the results of both experiments plotted against the models for the lumped parameters. Three whisker modules with different membrane materials, all silicone rubbers, were tested: EF10 (Ecoflex 0010), EF30 (Ecoflex0030), and MM30 (MoldMax 30) [19]. The material properties of the membranes were chosen to span a range of known FSC tissue properties and test the model's validity within that range. Fig. 3(a) shows measured torques versus the corresponding loading angles as the whisker was loaded (blue circles) and unloaded (red dots). The membrane elastic behavior showed no hysteresis.

TABLE I

FSC CHARACTERIZATION: FOR ALL MODULES $L = 0.17m$, $\ell = 0.018m$, $D = 0.012m$, AND $h = 0.005m$.

Module	$E_1(Pa)$	$\mu_1(Pas^{-1})$	$k_1(Nm)$	$b_1(Nm/rads^{-1})$
EF10	20×10^3	6	3.6	1.1×10^{-3}
EF30	40×10^3	3	7.3	3.6×10^{-4}
MM30	80×10^3	2	14.6	5.5×10^{-4}

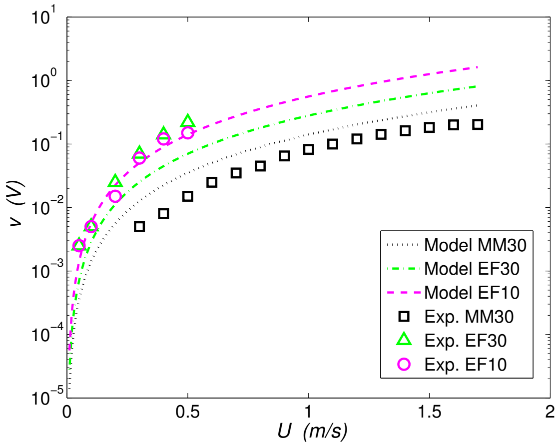

Fig. 5. Whisker as velocity sensor: measured sensor voltage v vs. towing speed U for threee different modules (colored markers) vs predicted performance based on (2) (colored dashed lines).

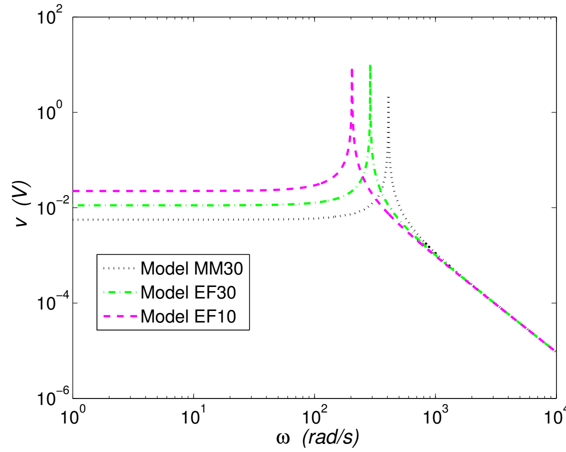

Fig. 6. Whisker frequency response: amplitude of predicted voltage v vs. signal frequency ω based on (3).

Fig. 3(b) shows measured damping coefficients (using (8)) for each membrane material versus predicted values (based on (5)). The whisker shafts used in all modules were made of polycarbonate. Table I lists material properties and dimensions of the modules tested as well as characterization results. The stiffness ratios, as defined in the previous section, were: $k^*_{EF10} = 10$, $k^*_{EF30} = 5$, and $k^*_{MM30} = 2.5$.

Sensor characterization

To characterize the sensor DC performance whisker modules were towed at constant speeds along the length of a 10m x 2m x 1.5m water tank. Fig. 4 shows the various experiment components. Fig. 4(a) shows a sample whisker module along with a close up of the whiskers used. The undulations, characteristic of pinniped whiskers, can be seen. Fig. 4(b) shows views of the carriage used to mount and tow whisker modules inside the tank. The same three whisker modules described earlier were tested. Fig. 5 shows sensor measurements v (volts) versus towing speed U (m/s) against model predictions using (2).

V. DISCUSSION

Previous studies on underwater whisker-like sensors have focused on micro scale sensors where the boundary layer of the surface where the sensors are mounted plays an important role in sensing dynamics. The large scale sensors described in this study extend past the boundary layer and the resulting fluid-structure interactions likely differ from fish neuromasts and arthropod filiform hairs. The results presented in the previous section demonstrate how the simple low order model in (1) can be used to describe the behavior of whisker-like mechanisms as flow velocity sensors. Two conditions must hold. Since elongated whisker-like bodies are susceptible to VIV, a potentially disruptive noise source, a mechanism must be in place to prevent vortex shedding from developing into full blown VIV. In this case the whisker shaft geometry mimics pinniped off-phase longitudinal axis undulations (Fig. 4(a)) which have been shown to minimize VIV [5]. In addition, the proper stiffness ratio between the whisker shaft and its supporting FSC defined in (7) prevents higher order modes from being excited. The whisker shaft can then be assumed to undergo pure rigid body oscillations and a simple damped oscillator model can effectively be used to describe the fluid-whisker-FSC interactions.

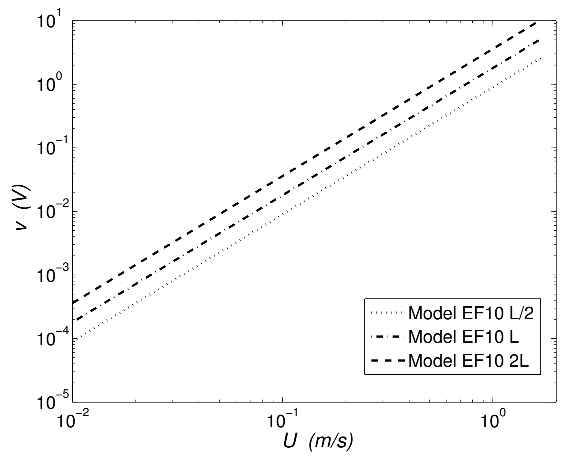

Fig. 7. Whisker as velocity sensor: predicted voltage v vs. towing speed U for three different whisker-shaft lengths based on (6).

In the biological system the FSC contains all mechanoreceptors and as a result sensing is done only at the base of the whisker shaft. The sensitivity of FSC nerve endings can potentially allow measurements of higher order modes along with the shaft's rigid body oscillations. In practice, the sensing elements presented here have that capability as well but the simplified approach presented herein enables sensing predictions that are accurate enough for control algorithms.

The FSC system identification employed base deflections θ of up to $0.27 rad$ and impulse responses where the sensors showed linear elastic behavior and low damping coefficients. The whisker-like sensors in this study are capable of detecting flow speeds spanning two orders of magnitude (ranging from $0.05m/s$ up to $2m/s$). Of the modules tested only EF10 presented a stiffness ratio an order of magnitude larger than unity, the other modules displayed values closer to unity. The low stiffness ratios should affect AC predictions (response resonant peaks, magnitudes, and phase) as higher modes could influence measurements when signal frequencies increase. DC measurements would suffer from steady state errors as whisker shafts would deform along with FSCs and absorb part of the inputs without measuring them. As expected, the DC model fit is best for EF10, while the model underestimates EF30 and overestimates MM30 behaviors. Still, predictions are overall qualitatively acceptable.

The whisker shafts used were made from polycarbonate and have similar moduli to real whiskers (keratin). The challenge to achieve low stiffness ratios is to find soft and durable membrane polymers. Membrane thickness also plays a role in sensor stiffness but softer membranes can also give way to large amplitudes that can saturate measurements. The practical stiffness ratio limit for these sensors seems to be in the order of 10, still modules with lower values can qualitatively follow the predictions found with our simple model.

Fig. 6 shows the estimated frequency response (amplitude) for the three modules. Since higher order modes might be excited in EF30 and MM30, several peaks can appear after the first resonance (the models only predict the first resonant frequencies). Finally, Fig. 7 shows predicted DC behavior for a module with $k^* = 10$ as the whisker scale is decreased by a factor of $\frac{1}{2}$ and increased by a factor of 2. Velocity measurement thresholds (what can be measured) increase with whisker size as expected from (6).

The minimum and maximum detectable flow speeds are determined primarily by the FSC material properties and the sensing mechanism. The stiffness ratio controls sensitivity and FSC deformation which plays a role in sensing mechanism selection. Small FSCs are preferred for array implementations (to allow tight packing of whiskers) but the follicle volume requires careful consideration as it limits the absolute whisker base rotation before saturation (when the whisker base runs into the follicle walls). The resistive sensors used for the experiments can be tuned by changing the value of their series resistance R_s. For $R_s = 1000\Omega$ the minimum velocity increment detectable is in the order of cm/s. Smaller follicle volumes would require more sensitive measurement transduction. Capacitive sensing elements could present a good alternative to the resistive elements currently used in applications where packaging is of concern (e.g. arrays).

VI. CONCLUSIONS

The dynamic behavior of a whisker-like sensor was described as well as the conditions for the analysis validity. In the absence of VIV, a simple forced oscillator model can accurately predict the sensor behavior both for continuous and oscillatory signals provided a stiffness ratio larger than unity is in place. The artificial FSC plays a central role in tailoring the sensor range and its sensitivity. The large scale sensors ($L = 0.17m$) used in this study showed sensitivities of $0.05m/s$ and were capable of measuring speeds of up to $2m/s$. Sensor natural frequencies can in principle be tailored to low pass filter environment signals and their readings can be used as feedback needed for navigation and tracking using local hydrodynamics. When using sensors with low stiffness ratios care must be taken that large frequency noise does not fall close to un-modeled high order resonant peaks. Future studies will address the effects of higher order whisker shaft modes on sensing as well practical field applications.

ACKNOWLEDGMENT

The authors would like to acknowledge A. Kottapalli, M. Asadniaye, and H. Hans for their help during material characterization and dynamic experiments.

REFERENCES

[1] L. Sarcione, Minimizing Current Effects on Autonomous Surface Craft Operations in Singapore Harbor, M.S., Dept. Mech. Eng., Mass. Inst. of Tech., Cambridge, MA, 2010.

[2] V. Fernandez, A. Maertens, F. Yaul, J. Dahl, J. Lang, and M. S. Triantafyllou. Lateral-line-inspired sensor arrays for navigation and object identification, *Marine Technology Society Journal*, Jul 2011.

[3] G. Dehnhardt, B. Mauck, W. Hanke, and H. Bleckmann, Hydrodynamic trail-following in harbor seals (Phoca vitulina), Science., 293, pp. 102-104, 2001.

[4] W. Hanke, M. Witte, L. Miersch, M. Brede, J. Oeffner, M. Michael, F. Hanke, A. Leder, and G. Dehnhardt, "Harbor seal vibrissa morphology suppresses vortex-induced vibrations," *J. Exp. Bio.*, 213, pp. 2665-2672, 2010.

[5] P. Valdivia y Alvarado, V. Subramaniam, and M.S. Triantafyllou, Design of a Bio-Inspired Whisker Sensor for Underwater Applications, Proc. IEEE Sensors, Taipei, Taiwan, 2012.

[6] J. Tao, and X. Yu. Hair flow sensors: from bio-inspiration to bio-mimicking-a review, *Smart Materials and Structures* , 21, 2012.

[7] Z.F. Fan, J. Chen, J. Zou, D. Bullen, C. Liu, and F. Delcomyn, Design and fabrication of artificial lateral line flow sensors, *J. Micromech. Microeng.*, 12, pp. 655-661, 2002.

[8] N. Nguyen, D.L. Jones, Y.C. Yang, and C. Liu, Flow vision for autonomous underwater vehicles via and artificial lateral line EURA-SHIP, *J. Adv. Signal. Process.*, 2011 806406.

[9] Y.C. Yang, A. Klein, H. Bleckmann, and C. Liu, Artificial lateral line canal for hydrodynamic detection, *Appl. Phys. Lett.*, 99 023701, 2011.

[10] J.J. Van Baar, M. Dijkstra, R.J. Wiegerink, T.S.J Lammerink, and, G.J.M Krijnen, Fabrication of arrays of artificial hairs for complex flow pattern recognition. Proc. IEEE Sensors, 2003, pp 332-336.

[11] M. Dijkstra, J.J. Van Baar, R.J. Wiegerink, T.S.J Lammerink, J.H. de Boer, and, G.J.M Krijnen, Artificial sensory hairs based on the flow sensitive receptor hairs of crickets. *J. Micromech. Microeng.*, 15, S132-8, 2005.

[12] N. Izadi, J.M. de Boer, J.W. Berenschot, and, G.J.M Krijnen, Fabrication of superficial neuromast inspired capacitive flow sensors. *J. Micromech. Microeng.*, 20, 085041, 2010.

[13] J.B. Stocking, W.C. Eberhardt, Y.A. Shakhsheer, and B.H. Calhoun, A Capacitance-based Whisker-like Artificial Sensor for Fluid Motion Sensing, Proc. IEEE Sensors, 2010.

[14] W.C. Eberhardt, Y.A. Shakhsheer, and B.H. Calhoun, A Bio-Inspired Artificial Whisker for Fluid Motion Sensing with Increased Sensitivity and Reliability, Proc. IEEE Sensors, 2011.

[15] J.H. Solomon, and M.J. Hartmann, Robotic whiskers used to sense features, *Nature*, 443, 2006.

[16] Author's unpublished measurements of Harbor Seal Whisker mechanical properties.

[17] B. Mitchinson, K.N. Gurney, P. Redgrave, C. Melhuish, A.G. Pipe, M. Pearson, I. Gilhespy, and T.J. Prescott, Empirically inspired simulated electro-mechanical model of the rat mystacial follicle-sinus complex, *Proc. R. Soc. Lond.* B 271, 2509-2516, 2004.

[18] Flexible displacement sensor: http://www.flexpoint.com

[19] Silicone rubbers: http://www.smooth-on.com